

Effects of surface roughness and wettability on bubble nucleation of water containing insoluble gas: A molecular dynamics study

Sicheng Zhang(张思程), Mian Yu(余绵), Bingheng Li(李丙衡), Lianxiang Ma(马连湘), and Yuanzheng Tang(唐元政)

Citation: Chin. Phys. B, 2026, 35 (**3**): 034701. DOI: 10.1088/1674-1056/ae3234
http://cpb.iphy.ac.cn; http://iopscience.iop.org/cpb

What follows is a list of articles you may be interested in

Molecular dynamics study incorporating regression analysis: Quantitative effects of sinusoidal protrusions and wettability on water phase transition containing insoluble gases

Bingheng Li(李丙衡), Yujian Gao(高雨键), Mian Yu(余绵), Lianfeng Wu(吴连锋), Lianxiang Ma(马连湘), and Yuanzheng Tang(唐元政)
Chin. Phys. B, 2025, 34 (**11**): 114704. DOI: 10.1088/1674-1056/ae0894

A molecular dynamics study of bubble nucleation on grooved surfaces: Effects of wettability and heat flux

Mian Yu(余绵), Bingheng Li(李丙衡), Lianfeng Wu(吴连锋), Lianxiang Ma(马连湘), Xiangwen Meng(孟祥文), and Yuanzheng Tang(唐元政)
Chin. Phys. B, 2025, 34 (**11**): 114703. DOI: 10.1088/1674-1056/ae0896

Stable nanobubbles on ordered water monolayer near ionic model surfaces

Luyao Huang(黄璐瑶), Cheng Ling(凌澄), Limin Zhou(周利民), Wenlong Liang(梁文龙), Yujie Huang(黄雨婕), Lijuan Zhang(张立娟), Phornphimon Maitarad, Dengsong Zhang(张登松), and Chunlei Wang(王春雷)
Chin. Phys. B, 2025, 34 (**1**): 014701. DOI: 10.1088/1674-1056/ad989d

Simulation of single bubble dynamic process in pool boiling process under microgravity based on phase field method

Chang-Sheng Zhu(朱昶胜), Bo-Rui Zhao(赵博睿), Yao Lei(雷瑶), and Xiu-Ting Guo(郭秀婷)
Chin. Phys. B, 2023, 32 (**4**): 044702. DOI: 10.1088/1674-1056/aca209

A study of cavitation nucleation in pure water using molecular dynamics simulation

Hua Xie(谢华), Yuequn Xu(徐跃群), and Cheng Zhong(钟成)
Chin. Phys. B, 2022, 31 (**11**): 114701. DOI: 10.1088/1674-1056/ac588a

---

SPECIAL TOPIC — Heat conduction and its related interdisciplinary areas

Effects of surface roughness and wettability on bubble nucleation of water containing insoluble gas: A molecular dynamics study

Sicheng Zhang(张思程), Mian Yu(余绵), Bingheng Li(李丙衡),
Lianxiang Ma(马连湘), and Yuanzheng Tang(唐元政)†

College of Electromechanical Engineering, Qingdao University of Science and Technology, Qingdao 266061, *China*

(Received 5 November 2025; revised manuscript received 22 December 2025; accepted manuscript online 31 December 2025)

As heat dissipation in micro- and nanoelectronic devices has become a critical bottleneck limiting performance improvement, microscale boiling has attracted increasing attention in recent years. Bubble nucleation in water containing nitrogen as an insoluble gas on copper surfaces with varying roughness and wettability is systematically investigated using molecular dynamics (MD) simulations. The results show that increasing surface roughness significantly enhances bubble nucleation by providing additional nucleation sites. The characteristic time of bubble nucleation in water containing insoluble gas decreases with reduced surface hydrophilicity, which differs markedly from previous MD studies of boiling in pure water. This finding suggests that enhanced adsorption of insoluble gas on hydrophobic surfaces facilitates bubble nucleation, in good agreement with experimental observations. These results provide valuable theoretical insights into microscale boiling heat transfer and offer guidance for optimizing thermal management in micro- and nanoelectronic systems.

Keywords: bubble nucleation, molecular dynamics, roughness, wettability, insoluble gas

PACS: 47.11.Mn, 47.55.dd, 68.35.Ct, 61.30.Hn

DOI: 10.1088/1674-1056/ae3234 **CSTR:** 32038.14.CPB.ae3234

1. Introduction

Boiling is a highly efficient heat transfer process that involves the rapid vaporization of a liquid above its saturation temperature and plays a crucial role in various applications, including energy conversion,[1] aerospace,[2,3] biomedical applications,[4–6] seawater desalination,[7–9] as well as everyday and industrial heating processes.[10,11] In particular, with the ongoing advancement of micro- and nanoelectronic devices toward higher integration and power density,[12–14] heat dissipation has become a critical bottleneck limiting further performance improvement. Among various cooling strategies, boiling heat transfer remains one of the most effective methods for dissipating high heat fluxes. Therefore, understanding bubble nucleation during nucleate boiling at the microscale is fundamentally important for improving boiling performance in micro- and nanoscale systems.

Many studies have explored the effects of surface roughness and wettability on bubble nucleation. While experimental studies focus on macroscopic observations, they do not reveal the underlying microscopic mechanisms. In contrast, molecular dynamics (MD) simulations offer detailed insights into bubble nucleation at the atomic scale. For example, Ahmad *et al.*[15] conducted MD simulations to investigate how the structure of nanobumps influences boiling heat transfer over the surface, finding that rectangular nanobumps exhibit the highest evaporation and heat transfer rates because of their larger solid–liquid interfacial area. Fallahzadeh *et al.*[16] studied how nanowall patterns influence boiling, showing that crossed nanowalls trigger the early onset of explosive boiling. Cao *et al.*[17] explored the role of surface roughness in bubble nucleation, finding that surface cavities stabilize nucleation sites and promote bubble nucleation, growth, and coalescence as roughness increases. Bai *et al.*[18] investigated the effect of surface wettability on boiling heat transfer and attributed the improved heat transfer performance on hydrophilic surfaces to their higher surface potential energy. Zhao *et al.*[19] observed bubble nucleation on grooved surfaces with hybrid wettability, revealing that all-hydrophilic grooves exhibit the fastest bubble growth rate. Wang *et al.*[20] found that hydrophobic regions on grooved surfaces prolong nucleation time. Liu *et al.*[21] discovered that superhydrophilic nanostructures enhance heat transfer. Yin *et al.*[22] demonstrated that nanofluids exhibit better boiling performance than base fluids and attributed this improvement to enhanced surface wettability and solid–liquid heat transfer efficiency resulting from nanoparticle deposition.

These MD studies, however, primarily focus on pure-fluid systems without considering the influence of insoluble gases. In such pure-fluid systems, a consensus has been established that hydrophilic surfaces generally promote boiling heat transfer because of their stronger solid–liquid interactions and lower interfacial thermal resistance (e.g., Bai *et al.*[18]

†Corresponding author. E-mail: tangyuanzheng@163.com

© 2026 Chinese Physical Society and IOP Publishing Ltd. All rights, including for text and data mining, AI training, and similar technologies, are reserved.

and Yin *et al.*[22]). The role of insoluble gases, which are ubiquitous in practical boiling systems, remains largely unexplored in MD simulations, especially in coupling with surface roughness and wettability. This knowledge gap is significant because insoluble gases can serve as pre-existing nucleation sites, potentially altering the nucleation mechanism and even reversing the conventional effect of surface wettability observed in pure-fluid systems.

Despite these findings, most studies focus on surface roughness or wettability alone, and their combined effects have not been systematically explored. Moreover, the influence of insoluble gases, which are critical in boiling processes, is rarely considered in MD studies. In this work, grooved surfaces with varying roughness and wettability are designed by adjusting the period of sinusoidal grooves and modifying the interactions between water molecules and copper atoms. To better simulate realistic conditions, a constant heat flux method is used to heat the copper substrate and induce bubble nucleation, with N_2 introduced as the insoluble gas. Building on these approaches, the combined effects of surface roughness, wettability, and the presence of insoluble gas are systematically investigated. The results show that bubble nucleation accelerates with increasing surface roughness and decreasing surface hydrophilicity. Additionally, analyses of density distribution, interfacial thermal resistance, and temperature variation are conducted to provide insights into the underlying mechanisms.

2. Simulation methods

As shown in Fig. 1(a), the simulation system is a rectangular box composed of four components: an upper copper (Cu) plate, a bottom Cu plate, H_2O molecules between the plates, and N_2 molecules in the water. The system contains a total of 25989 atoms and has dimensions of 122.69 Å, 20.00 Å, and 520.00 Å along the x, y, and z directions, respectively. Specifically, along the z direction, the fixed bottom Cu plate has a height of 34.4 Å, the liquid water film is 116.7 Å thick, and the movable upper Cu plate has a height of 123.4 Å. The Cu atoms are arranged in a face-centered cubic (FCC) lattice with a lattice constant of 3.61 Å. The bottom Cu surface is contoured into a sinusoidal waveform, described by the function

$$f(x) = h_0 + A\sin(2\pi x/p), \tag{1}$$

where h_0 is the distance from the surface to the z axis, A is the amplitude, and p is the period.[23] The sinusoidal grooves are modeled on the bottom Cu plate, which consists of 6 atomic layers. Specifically, the bottom-most 3 Cu atomic layers are fixed to prevent deformation and displacement of the heated surface, while the next 3 layers are used to apply heat flux, serving as the heat source of the system. As shown in Fig. 1(b), the sinusoidal grooves repeat from 1 cycle to 5 cycles, with surface roughness increasing as the period p increases. To ensure consistent comparison across different roughness conditions, the width d and the height h of the grooved structures are kept constant in all models. The numbers of H_2O and N_2 molecules remain constant at 6679 and 60, respectively, in all models. At 298 K and 1 atm, the solubility of nitrogen gas in water is approximately 1.2×10^{-5} mol·mol^{-1}.[24] Given this low solubility, fewer than one N_2 molecule can dissolve in 6679 H_2O molecules, indicating that the N_2 molecules remain in the gas phase and are effectively insoluble.

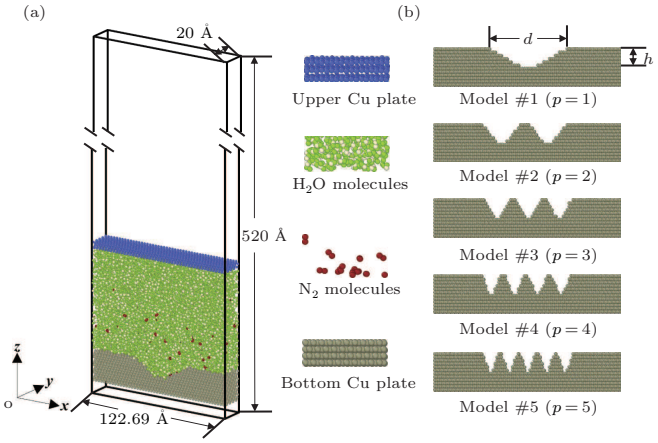


Fig. 1. Initial configuration of the simulation domain.

The bottom Cu substrate is continuously heated during the simulation. To prevent the collapse of the sinusoidal grooves while ensuring that all Cu atoms vibrate solely around their equilibrium sites, an elastic restoring force is imposed on each Cu atom in the system[25]

$$F = -K\cdot r. \tag{2}$$

Here, $K = 52$ N·m^{-1} is the elastic constant, and r is the displacement of an atom relative to its initial position.

The interaction between Cu atoms is represented by the van der Waals (vdW) force, described by the Lennard–Jones (L–J) potential[26]

$$\Phi_{(r_{ij})} = 4\varepsilon\left[\left(\frac{\sigma}{r_{ij}}\right)^{12} - \left(\frac{\sigma}{r_{ij}}\right)^{6}\right], \quad r_{ij} \le r_{\text{cut}}, \tag{3}$$

where ε and σ are the energy and distance parameters, respectively. The distance between atoms i and j is denoted by r_{ij}, and r_{cut} is the cutoff radius. Van der Waals interactions for H_2O–Cu, H_2O–N_2, and Cu–N_2 pairs are represented by O–Cu, O–N, and Cu–N interactions, respectively. The SPC/E model[27,28] is employed for water molecules, effectively capturing their physical and chemical properties while balancing computational accuracy and efficiency. In this model, the atomic charges are $q_{\text{O}} = -0.8476e$ and $q_{\text{H}} = 0.4238e$. The SHAKE algorithm[29] is applied to constrain the O–H bonds and the H–O–H angle, thereby reducing computational cost.

Long-range electrostatic interactions are computed using the particle–particle particle–mesh (PPPM) solver,[30] with intermolecular forces between H_2O molecules primarily described by O–O interactions. For diatomic N_2 molecules, intramolecular and intermolecular interactions are parameterized using the OPLS-AA/L force field.[31,32] Surface wettability is modulated by adjusting the L–J potential parameters of O–Cu interactions, as specified below:

$$\Phi_{(r_{ij})} = 4\varepsilon' \left[\left(\frac{\sigma'}{r_{ij}} \right)^{12} - \left(\frac{\sigma'}{r_{ij}} \right)^{6} \right], \tag{4}$$

$$\varepsilon' = \beta^2 \varepsilon, \tag{5}$$

$$\sigma' = \beta^{-1/6} \sigma. \tag{6}$$

where β serves as a scaling factor to modulate wettability, and ε' and σ' denote the modified energy and length parameters, respectively. The L–J potential parameters used in this study are listed in Table 1. The water contact angles on hydrophobic, neutral, and hydrophilic surfaces, calculated using a cylindrical droplet MD model, are 120.0°, 87.3°, and 4.7°, respectively.

Table 1. L–J potential parameter.

Atom pairs	σ (nm)	ε (meV)
Cu–Cu[26]	0.2338	409.330
O–O[27,28]	0.3166	6.739
N–N[31,32]	0.3250	3.368
O–Cu (neutral)[33,34]	0.3190	7.370
O–Cu (hydrophobic)	0.3380	3.685
O–Cu (hydrophilic)	0.3011	14.740
O–N	0.3208	4.764
Cu–N	0.2794	37.130

Periodic boundary conditions are applied in the x and y directions. In the z direction, the system is confined between two solid copper walls: the fixed bottom substrate at the negative z extreme and the movable upper plate at the positive z extreme. This configuration allows implementation of the piston-based pressure control method described below. To maintain a stable pressure throughout the simulation, a piston-based pressure control method is employed.[35] Central to this approach is the configuration of the upper copper plate as a movable piston. An external force is applied in the z direction to each atom of this piston, thereby achieving dynamic pressure balance within the system. This design effectively mitigates pressure fluctuations that could interfere with bubble nucleation, ensuring the accuracy and stability of the simulation and providing reliable data for subsequent analysis. The force on each atom in the upper plate is calculated using the following equation:

$$F_{\text{atom}} = \frac{F_{\text{total}}}{N_{\text{up}}} = \frac{P \cdot S_{xoy}}{N_{\text{up}}}, \tag{7}$$

where F_{total} represents the total force acting on the upper Cu plate, N_{up} is the number of atoms constituting the plate, the target pressure P is set to 1 bar, and S_{xoy} denotes the cross-sectional area in the xoy plane.

The MD simulation in this study is divided sequentially into two main stages: the relaxation stage and the heating stage. The relaxation stage involves equilibrating the entire simulation system (excluding the bottom frozen Cu atoms) under the canonical (NVT) ensemble. During this stage, the initial system is run at a constant temperature of 298 K for 1 ns, with temperature controlled by the Langevin method,[36] ensuring that H_2O molecules reach a stable adsorption configuration on the Cu substrate. During the heating stage, the equilibrated system is simulated under the microcanonical (NVE) ensemble.

A constant heat flux of 1.97×10^{10} W·m^{-2} is applied to the Cu substrate in all simulated cases to trigger bubble nucleation. External heat is uniformly applied to each copper atom within the hot reservoir using an asymmetric version of the enhanced heat exchange algorithm. To further analyze the dynamic behavior of bubbles during heating, atomic temperature, density trajectory data, and upper plate displacement data are collected every 1 ps, comprehensively recording the bubble formation process.

The integration of the equations of atomic motion is performed with a time step of 1 fs using the large-scale atomic/molecular massively parallel simulator (LAMMPS).[37] VMD[38] and OVITO[39] are used for visualization and data analysis.

3. Results and discussion

Bubble nucleation is analyzed through the evolution of atomic trajectories. As shown in Fig. 2, bubble nucleation initiates at the solid–liquid interface, with two distinct types of nucleation sites identified. One type of favorable nucleation site is located inside the groove, where high superheat conditions exist because of proximity to the heat source. The other type is located at the adsorption sites of N_2 molecules on the substrate, consistent with the gas adsorption layer theory.[40,41] The bubble nucleation process within the groove follows a distinct pattern. On surfaces with a single groove (i.e., Model #1 in Figs. 2(a)–2(c)), bubble nucleation begins inside the groove and grows to occupy the groove mouth. This process continues as the bubble enlarges, with the three-phase contact line moving away from the groove edge. Eventually, a vapor film forms above the surface, pushing the water nanofilm away. In contrast, on surfaces with multiple continuous grooves (i.e., Model #3 in Figs. 2(d)–2(f) and Model #5 in Figs. 2(g)–2(i)), bubble nucleation occurs separately within each groove. Once each bubble occupies the mouth of its respective groove, coalescence occurs, forming a larger bubble that extends across the junction between the grooved and planar areas of the surface. Subsequently, similar to surfaces with a single groove,

a vapor film forms as the larger bubble grows. Surfaces with two or four grooves exhibit similar bubble nucleation behavior and are therefore not shown here.

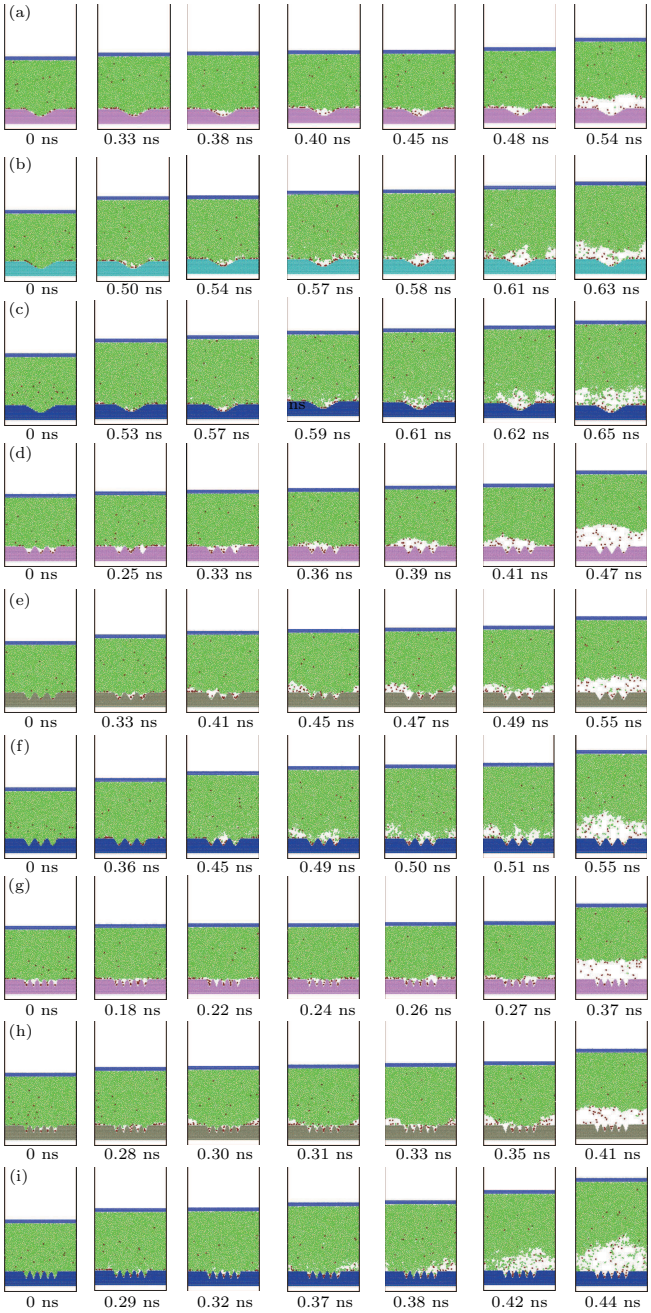


Fig. 2. Snapshots of atomic trajectories at representative time points. Model #1: A single groove on surfaces with (a) hydrophobic, (b) neutral, and (c) hydrophilic wettability. Model #3: Three continuous grooves on surfaces with (d) hydrophobic, (e) neutral, and (f) hydrophilic wettability. Model #5: Five continuous grooves on surfaces with (g) hydrophobic, (h) neutral, and (i) hydrophilic wettability.

Moreover, the atomic trajectories reveal the effects of surface roughness and wettability on bubble nucleation rates. Based on the bubble behaviors described above, two key time points are used to characterize the bubble nucleation rate. The first corresponds to the moment when a bubble on single-grooved surfaces, or a coalesced bubble on multiple-grooved surfaces, occupies the mouth of the groove(s) (referred to in the literature as the nucleation cavity state). The second corresponds to the formation of a continuous vapor film above the surface. The characteristic times, namely the nucleation cavity state time and the vapor film formation time, are plotted in Fig. 3. It is observed that bubble nucleation accelerates with increasing surface roughness, whereas it slows down with increasing surface hydrophilicity.

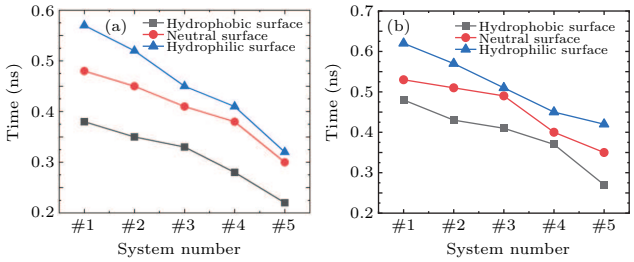


Fig. 3. Characteristic times of bubble nucleation: (a) nucleation cavity state time and (b) vapor film formation time.

The increase in bubble nucleation rate with increasing surface roughness is in good agreement with previous MD studies.[15–17] However, the decrease in bubble nucleation rate with increasing surface hydrophilicity conflicts with previous MD studies focusing on the effect of wettability on the boiling of pure fluids without insoluble gas.[18–22] This suggests that the presence of insoluble gas significantly affects bubble dynamics. To uncover the underlying mechanisms, the density distribution, N_2 adsorption on surfaces, interfacial thermal resistance (ITR), and temperature variation are analyzed in detail.

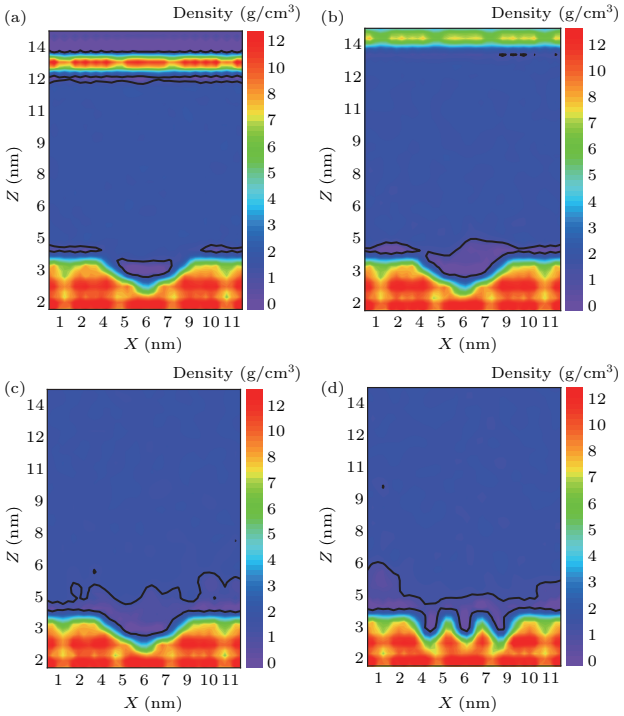


Fig. 4. Density distribution diagrams at specific time points for cases with different surface roughness and wettability conditions: (a) Model #1, hydrophobic, 0.45 ns; (b) Model #1, neutral, 0.51 ns; (c) Model #1, hydrophilic, 0.61 ns; (d) Model #3, hydrophilic, 0.5 ns.

As shown in Fig. 4, bubble nucleation occurs adjacent to the bottom substrate. For Model #1 with a hydrophobic surface (Fig. 4(a)), distinct low-density regions appear above the substrate surface as early as 0.45 ns, resulting from preferential bubble nucleation and rapid growth in these regions. Additionally, the bubbles exhibit a flattened shape due to the hydrophobic nature of the surface, which reduces the adhesion force of liquid H_2O molecules and lowers the nucleation energy barrier.[42,43] For Model #1 with neutral and hydrophilic surfaces, the low-density regions form at 0.51 ns and 0.61 ns, as illustrated in Figs. 4(b) and 4(c), respectively. It is observed that the low-density area enlarges with increasing surface hydrophilicity. Furthermore, separate bubble nucleation sites inside the grooves are observed as multiple discrete low-density regions, as shown in Fig. 4(d).

To further elucidate the significant role of insoluble N_2 molecules in bubble nucleation, the temporal evolution of the number of N_2 molecules within a 20 Å layer from the bottom of the groove is quantified, as shown in Fig. 5. The number of N_2 molecules in the selected regions increases with increasing surface roughness, which is attributed to additional adsorption sites available for N_2. In contrast, the number of N_2 molecules decreases with increasing surface wettability because of competitive adsorption between H_2O and N_2 molecules on the substrate surface. Two distinct stages are observed in the evolution of N_2 molecules: an initial increasing stage followed by a rapid decreasing stage. The initial increase in N_2 molecules is driven by enhanced gas diffusion as the system temperature rises. Once a continuous vapor film forms over the substrate (i.e., complete drying of the surface), the external heat flux further heats the substrate, leading to a rapid decline in the number of N_2 molecules. Since N_2 clusters act as pre-existing nucleation sites, surfaces with higher roughness and weaker wettability exhibit superior bubble nucleation performance.

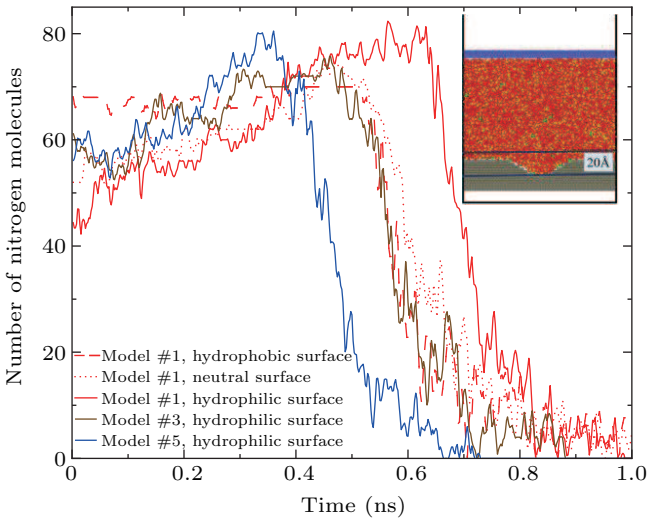


Fig. 5. Temporal evolution of the number of N_2 molecules within a 20 Å layer from the bottom of the groove.

The heat transfer from the bottom Cu plate to the liquid film is the primary driving force for bubble nucleation. Although a constant heat flux is applied, the interfacial heat transfer efficiency is regulated by wettability. Consequently, to quantitatively compare the effect of wettability, the interfacial thermal resistance (ITR) at the solid–liquid interface between the bottom plate and adjacent water was calculated, with its temporal evolution shown in Fig. 6. The ITR is calculated using the Kapitza formula[44]

$$R_{\mathrm{K}} = \frac{T_2 - T_1}{q}, \tag{8}$$

where T_2 is the average temperature of the top three layers of Cu atoms at the bottom plate, T_1 is the average temperature of the liquid H_2O in the selected region (the 20 Å-thick layer shown in Fig. 5), and q is the heat flux from the heat source.

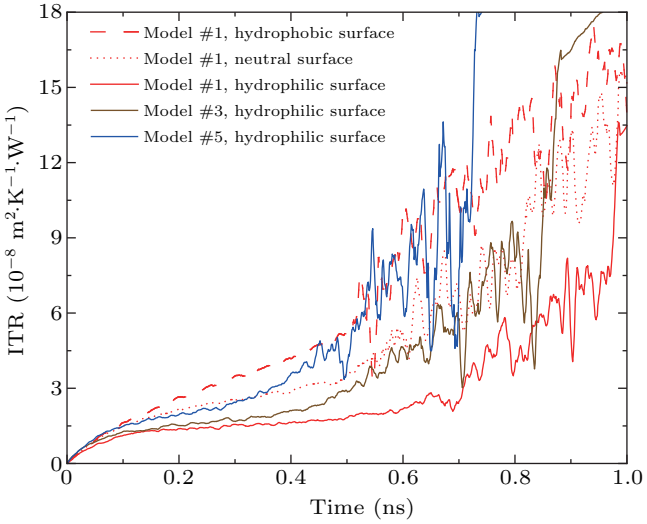


Fig. 6. Temporal evolution of solid–liquid ITR.

As shown in Fig. 6, the ITRs are compared between surfaces with different roughness and wettability conditions. In line with previous MD studies,[18,22] the ITR decreases with increasing surface hydrophilicity. However, the impact of ITR on boiling performance in the present study contrasts with earlier findings. Previous MD studies suggest that lower ITR, achieved by hydrophilic surfaces, enhances heat transfer from the superheated solid to the liquid, which raises the liquid temperature near the solid surface and facilitates bubble nucleation. In contrast, the present work shows that hydrophobic surfaces, with higher ITR, exhibit better bubble nucleation performance. It should be noted that while lower ITR reflects higher heat transfer efficiency across interfaces, the apparent discrepancy between previous studies and the present work arises from methodological differences. In previous MD studies, the temperature of the solid substrate is controlled by a thermostat, and the heat flux from the solid substrate to the liquid is the response. In the present work, however, the heat flux is fixed, and the temperature difference between the solid and liquid serves as the response. Compared to hydrophilic

surfaces, the less efficient heat transfer across a hydrophobic surface causes thermal accumulation and a corresponding rise in substrate temperature, which enlarges the temperature difference between the substrate and the liquid. With the presence of insoluble gas, bubble nucleation is favored at the solid–liquid interface. Therefore, hydrophobic surfaces, with their higher temperature, facilitate bubble nucleation more effectively than hydrophilic surfaces. This observed reversal of the wettability effect — where hydrophobic surfaces promote nucleation despite their higher ITR — signals a fundamental shift in the dominant nucleation mechanism compared to pure-fluid systems. In MD studies of pure-water boiling (e.g., Bai *et al.*[18] and Yin *et al.*[22]), nucleation is predominantly a heat-transfer-limited process. Hydrophilic surfaces, with their stronger solid–liquid interaction and lower ITR, enable more efficient heat injection into the liquid, leading to earlier vaporization and nucleation. In contrast, the presence of insoluble N_2 in our system introduces a cavitation-driven mechanism. As quantified in Fig. 5, hydrophobic surfaces adsorb significantly more N_2 molecules, which serve as pre-existing, stable gas cavities. These cavities drastically reduce the energy barrier for bubble formation. Consequently, nucleation becomes primarily gas-availability-limited. Although the higher ITR of hydrophobic surfaces impedes heat transfer (Fig. 6), the overwhelming advantage of abundant gas nucleation sites, coupled with localized heat accumulation (resulting from that same higher ITR), leads to earlier nucleation. This paradigm shift from a thermal-dominant to a cavitation-dominant mechanism explains the apparent contradiction with prior pure-fluid studies and underscores the critical role of insoluble gas in modulating surface-wettability effects. As the bubble evolves, the ITR exhibits dynamic changes at different stages: it increases slightly during initial bubble nucleation and rises sharply upon the formation of a vapor film. Once a continuous vapor film forms, the ITR becomes irrelevant due to the sharp decrease in H_2O molecules in the selected region.

To gain deeper insight into the bubble nucleation mechanism at the solid–liquid interface, the temperature variation of the copper substrate within the selected region was investigated. The results show that adsorption of nitrogen on the surface reduces interfacial heat transfer efficiency, leading to thermal accumulation and a temperature rise at the bottom copper substrate, which in turn promotes bubble nucleation at this location. As shown in Fig. 7, a more pronounced temperature increase of the copper substrate is observed on surfaces with higher roughness and weaker wettability, further confirming the mechanism of gas adsorption–thermal accumulation–nucleation enhancement described above.

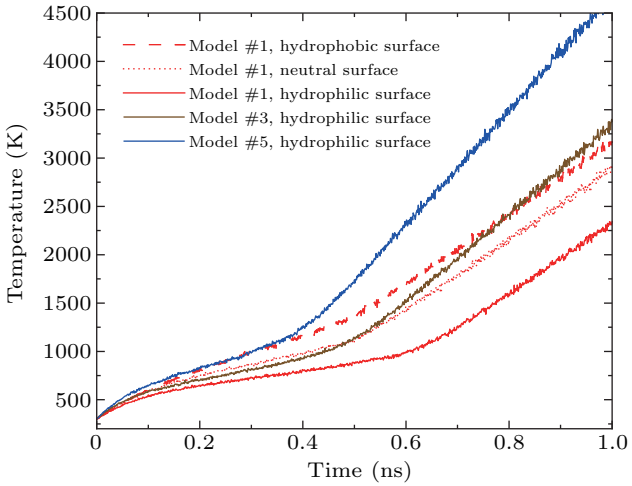


Fig. 7. Temperature change of the bottom copper plate.

4. Conclusion

This study investigated the effects of surface roughness and wettability on the nucleation and growth of bubbles during water boiling on a copper substrate, with a special focus on the presence of insoluble gas. The main findings are summarized as follows:

(i) Surface roughness effects: Under constant wettability, increasing surface roughness significantly enhances bubble nucleation through a dual mechanism. The enlarged effective heat transfer area improves thermal transfer into the liquid phase, leading to a faster temperature rise in the liquid adjacent to the solid substrate. Simultaneously, groove-rich structures provide additional nucleation sites, facilitating cooperative bubble growth and rapid coalescence, which effectively shortens nucleation time.

(ii) Wettability effects: Under constant roughness, wettability modulates the nucleation process by influencing the heat transfer efficiency at the solid–liquid interface. The less efficient solid–liquid heat transfer of hydrophobic surfaces leads to localized heat accumulation and the formation of pronounced superheated zones, resulting in an earlier onset of bubble nucleation.

(iii) Role of insoluble gas: This study incorporated N_2 molecules to mimic the role of insoluble gases in real systems. It was found that N_2 adsorption on the Cu substrate creates natural cavitation sites, which serve as stable nuclei for bubble formation, thereby enhancing nucleation capability and accelerating bubble generation. These results are consistent with macroscopic observations of bubble nucleation to some extent.

Thus, surface roughness and wettability collectively optimize the availability and stability of gas-based nucleation sites, fundamentally shifting the nucleation mechanism. This synergistic effect explains the superior performance compared to any single-factor modification.

Acknowledgment

This project was supported by the National Natural Science Foundation of China (Grant No. 52176077).

References

[1] Khan M S, Wood D A, Qyyum M A, Ansari K B, Ali W, Wazwaz A and Dutta A 2022 *J. Nat. Gas Sci. Eng.* **101** 104539
[2] Qiu H J, Qiu J S, Liu B Y, Yi X L and Wang K B 2013 *Appl. Mech. Mater.* **419** 616
[3] Ranganayakulu C and Kabelac S 2015 *J. Heat Transfer* **137** 121002
[4] Mondal N, Dutta S, Chatterjee S, Sarkar J, Mondal M, Roy C, Chakraborty R and Ghosh W 2024 *PLoS One* 19 e0310595
[5] Yang Z, Jiang X, Zhang T, Zhang X, Xie L, Li J, Ma L, Wang H and Chang Y 2024 *Fuel* **360** 130489
[6] Pryakhin E A, Urutskoev L I, Akleyev A V, Tryapitsyna G A and Deryagin P S 2023 *Nucl. Eng. Technol.* **55** 4204
[7] Iskander J, Shihimi O, El Mahallawy N and Abd-Elhady M 2024 *Discov. Water* **4** 3
[8] Chinnappan T and Raguraman C 2023 *Int. J. Ambient Energy* **44** 2047
[9] Kuznetzov Y, Romenkov A and Mishanina Y 2004 *Int. J. Nuclear Desalination* **1** 346
[10] Chen Y M, Hu N, Zhang J Y, Sun Y F, Wu Y F, Li Z R and Fan L W 2025 *Adv. Sci.* **12** 2413142
[11] Cao K, Song X, Qin F, Wei X and Li W 2025 *Appl. Therm. Eng.* **260** 125032
[12] Hou J, Wu J, Zhao X, Ma L, Huang L, Qiu Y, Li D, Ding Z, Chen Z and Wei J 2024 *Case Stud. Therm. Eng.* **58** 104458
[13] Birbarah P, Gebrael T, Foulkes T, Stillwell A, Moore A, Pilawa-Podgurski R and Miljkovic N 2020 *Int. J. Heat Mass Transfer* **147** 118918
[14] Wan Z P, Pi P H, Fu Y Q and Tang Y 2008 *J. Cent. South Univ. Technol.* **15** 235
[15] Ahmad S, Cheng H, Ali Z, Deng W, Lau K T, Ali H M and Zhao J 2024 *Int. Commun. Heat Mass Transfer* **153** 107329
[16] Fallahzadeh R, Bozzoli F, Cattani L and Azam M W 2024 *Energies* **17** 1107
[17] Cao Q, Li Z and Cui Z 2023 *Langmuir* **39** 12754
[18] Bai P, Wang D J and Liu Y F 2024 *Acta Phys. Sin.* **73** 090201 (in Chinese)
[19] Zhao H, Zhou L and Du X 2021 *Int. J. Heat Mass Transfer* **166** 120752
[20] Wang J, Yang M, Jia Y, Cui X and Chang H 2025 *Int. Commun. Heat Mass Transfer* **163** 108751
[21] Liu H, Yang S, Mei X, Li K, Xie Y and Lu L 2025 *Int. J. Heat Mass Transfer* **239** 126529
[22] Yin X, Hu C, Bai M and Lv J 2019 *Int. J. Multiph. Flow* **115** 9
[23] Yastrebov V A, Anciaux G and Molinari J F 2014 *Tribol. Lett.* **56** 171
[24] Kaye G W C and Laby T H 1986 *Tables of Physical and Chemical Constants*, (5th edn.) (New York: Longman) pp. 219
[25] Deng W, Ma S, Li W, Liu H and Zhao J 2022 *Int. J. Heat Mass Transfer* **191** 122856
[26] Yu J and Amar J G 2002 *Phys. Rev. Lett.* **89** 286103
[27] Berendsen H J, Grigera J R and Straatsma T P 1987 *J. Phys. Chem.* **91** 6269
[28] Kusalik P G and Svishchev I M 1994 *Science* **265** 1219
[29] Ryckaert J P, Ciccotti G and Berendsen H J 1977 *J. Comput. Phys.* **23** 327
[30] Hockney R W and Eastwood J W 2021 *Computer Simulation Using Particles* (Boca Raton: CRC Press)
[31] Jorgensen W L, Maxwell D S and Tirado-Rives J 1996 *J. Am. Chem. Soc.* **118** 11225
[32] Kaminski G A, Friesner R A, Tirado-Rives J and Jorgensen W L 2001 *J. Phys. Chem. B* **105** 6474
[33] Rafiee J, Mi X, Gullapalli H, Thomas A V, Yavari F, Shi Y, Ajayan P M and Koratkar N A 2012 *Nat. Mater.* **11** 217
[34] Pham A T, Barisik M and Kim B H 2016 *Int. J. Heat Mass Transfer* **97** 422
[35] Guo C, Ji C, Kong Y, Liu Z, Guo L and Yang Y 2023 *Mater.* **16** 1984
[36] Schneider T and Stoll E 1978 *Phys. Rev. B* **17** 1302
[37] Plimpton S 1995 *J. Comput. Phys.* **117** 1
[38] Humphrey W, Dalke A and Schulten K 1996 *J. Mol. Graph.* **14** 33
[39] Stukowski A 2009 *Modell. Simul. Mater. Sci. Eng.* **18** 015012
[40] Yang H, Xing Y, Zhang F, Gui X and Cao Y 2024 *Fundamental Res.* **4** 35
[41] Yang H, Xu M, Xing Y, Gui X and Cao Y 2025 *Acta Phys. Sin.* **74** 024702 (in Chinese)
[42] Sun Y, Zhang Z, Zhang G, Jiang Y and Zheng J 2025 *Int. J. Heat Mass Transfer* **241** 126729
[43] Li Y, Zhou W, Zhang Y, Qi B and Wei J 2020 *Int. Commun. Heat Mass Transfer* **119** 104991
[44] Liu Z, Liu Z and Liu R 2023 *Int. J. Therm. Sci.* **192** 108424